Ab Initio Calculation of the Miscibility Diagram for Hydrogen-Helium Mixtures

Manuel Schöttler[*] and Ronald Redmer

Institut für Physik, Universität Rostock, D-18051 Rostock, Germany

We use finite-temperature density functional theory coupled to classical molecular dynamics simulation to calculate the miscibility gap of hydrogen-helium mixtures. The van der Waals density functional (vdW-DF) theory is used, which leads to lower demixing temperatures compared to computations using the Perdew-Burke-Ernzerhof functional. Our calculations suggest that current Jupiter models are most likely too hot to allow demixing in the interior. A Jupiter isentrope based on our vdW-DF data is presented. Our demixing phase diagram still predicts phase separation in Saturn, but in a significantly reduced fraction of its volume.

Introduction.—Giant gas planets like Jupiter and Saturn contain mostly hydrogen and helium [1,2]. It has long been proposed that hydrogen and helium phase separate in the deep interior of Jupiter and Saturn, causing the formation of He-rich droplets that then sink towards the planetary core [3]. Strong indications for this process came from space missions that measured the He mass fraction Y in the atmosphere of Jupiter and Saturn. In Jupiter, the Galileo entry probe found a value of $Y_J = 0.238 \pm 0.005$ [2]. For Saturn, no entry probe data are available to date but the atmospheric He mass fraction was inferred from Voyager spectroscopic measurements that determined a value of $Y_S = 0.18$–0.25 [4]. The available data for both planets show a He depletion compared to the protosolar value of $Y = 0.28$ [5]. The precipitation of He would explain Saturn's excess luminosity [6–8] where the sinking droplets convert gravitational energy to heat, which contributes to the luminosity and delays the cooling of the planet. Models neglecting this process consistently fail to describe the thermal evolution of Saturn and yield a time duration of only 2–3 Gyr until its present luminosity is reached, much less than the solar age of 4.56 Gyr [9]. Additionally, the depletion of neon in Jupiter [10] is believed to be tied to He rain because Ne was found to dissolve preferably in the nonmetallic helium rather than in the metallic hydrogen [11]. Still, experiments have not been able to verify demixing under these extreme conditions. Thus, for the quantitative assessment of planetary models and evolution we rely on theoretical predictions that determine the thermodynamic conditions under which hydrogen and helium become immiscible.

Density functional theory (DFT) has become an important tool to study matter under planetary conditions. Several studies on the miscibility gap using DFT have been published [12–15]. Lorenzen *et al.* [14] studied the miscibility gap with DFT coupled to molecular dynamics using the Perdew-Burke-Ernzerhof (PBE) exchange-correlation

(XC) functional and the ideal entropy of mixing. Morales *et al.* [15,16] additionally calculated the nonideal entropy of H-He mixtures with a coupling-constant integration technique and found significantly smaller demixing temperatures compared to those of Lorenzen *et al.* Both demixing phase diagrams have been used to calculate the inhomogeneous evolution of Saturn and a better agreement with the solar age was found when the demixing temperatures were artificially lowered [8].

In DFT calculations the choice of the XC functional is of crucial importance, which, in principle, has to be validated against high precision measurements. Experiments by Knudson *et al.* [17] on deuterium showed that the metallization pressure in the liquid phase is not adequately described in DFT by using the PBE functional. The van der Waals density functional (vdW-DF) by Dion *et al.* [18] and the related vdW-DF2 [19] achieve better agreement with the experiment, because metallization is shifted to higher densities and pressures. It has been suggested that metallization of the hydrogen subsystem triggers the H-He immiscibility [20]. Thus, an XC functional that describes the metallization more accurately would also improve the miscibility diagram. Although the vdW-DF is more in agreement with the experiments of Knudson *et al.* [17], it disagrees with experiments by Ohta *et al.* [21] and Zaghoo *et al.* [22], and the recent quantum Monte Carlo (QMC) study by Mazzola *et al.* [23]. In Ref. [24] Knudson and Desjarlais report on Hugoniot and reshock experiments on deuterium where the vdW-DF predicts the onset of metallization best while the pressure width over which dissociation occurs is better described by PBE. A theoretical study on hydrogen-helium mixtures has been done by Clay *et al.* [25] who performed QMC calculations to benchmark many DFT XC functionals. They found that PBE is not able to capture the enthalpy of H-He mixtures, which is the key quantity in determining phase equilibria. The vdW-DF performs best with respect to enthalpies, yet the pressure

shows a larger error than PBE. Because of the high precision measurements by Knudson *et al.* and the benchmarking study by Clay *et al.* we conclude that the vdW-DF is better suited for the study of phase separation in hydrogen-helium mixtures so we present in this work the first vdW-DF miscibility diagram.

Methods.—Demixing was calculated by evaluating the free enthalpy (or Gibbs free energy) of mixing ΔG,

$$\Delta G(x,p,T) = G(x,p,T) - xG(1,p,T) - (1-x)G(0,p,T), \quad (1)$$

where G is the free enthalpy as a function of helium number fraction x, pressure p, and temperature T,

$$G(x,p,T) = U(x,p,T) - TS(x,p,T) + pV(x,p,T), \quad (2)$$

where U is the internal energy, V is the volume, and S is the entropy. We followed the approach of Lorenzen *et al.* [14], who fitted the free enthalpy of mixing using a Redlich-Kister ansatz [26] and applied a common tangent construction to ΔG to determine the helium fractions of the helium-poor and helium-rich phase. Equation (1) requires the first term on the right-hand side to be the free enthalpy of a perfectly mixed system. It has been shown [20,27] that demixing occurs directly in the simulation box if particle numbers are sufficiently high. From this, one could determine the thermodynamic states, for which demixing occurs, and the fractions in the He-rich and He-poor phase, but it is unclear how these properties converge with system size. Additionally, the demixed system would change the free enthalpy so that it eventually differs from the enthalpy of a uniformly mixed system. Thus, Eq. (1) would be inapplicable. To avoid these problems, we use relatively small particle numbers that ensure sufficiently mixed states in our simulations.

Density functional theory.—Finite-temperature density functional theory simulations coupled to classical molecular dynamics simulations (FT-DFT-MD) were performed with the VASP code [28–32], using the projector augmented wave (PAW) method [33] and the nonlocal vdW-DF of Dion *et al.* [18]. The internal energy U and pressure p were calculated as a function of helium concentration x, temperature T, and volume V. A constant electron number of 64 was used for all helium fractions. The resulting relatively small number of atoms ensures that the system remains fully mixed at all temperatures, pressures, and helium fractions considered. A plane-wave cutoff of 1200 eV and the Baldereschi mean-value [34] **k** point was used to obtain energies and pressures that were converged within 1%. Convergence tests with respect to electron number were carried out for pure H and He, where deviations have been less than 1% in the relevant pressure range. The Nose-Hoover thermostat [35] has been used and averages of pressure and energy have been taken for at least 10 000

time steps (2 ps) after thermodynamic equilibrium was reached. Calculations on the equation of state (EOS) were performed for 15 temperatures from 1000 to 15 000 K, several pressures in the range of 0.2–30 Mbar, and 31 He concentrations summing up to more than 7000 FT-DFT-MD simulations.

We correct our equation of state data for nuclear quantum effects (NQE) by applying the correction formulas of Ref. [36]. These corrections are weighted integrations over the spectral density of states, where the weighting function corresponds to the difference of a quantum harmonic oscillator to a classical one. This approach captures most of the quantum effects, but treats anharmonic contributions in the spectral density of states as being harmonic. In general NQE are only important for low temperatures while anharmonic effects become important for high temperatures.

The nonideal entropy was calculated by a combination of thermodynamic integration over the EOS [37] and coupling-constant integration (CCI) [16,38]. Thermodynamic integration allows the computation of entropies at arbitrary pressures and temperatures if a thermodynamic consistent EOS is available and if the entropy at a given reference EOS point is known. This reference entropy was calculated by the CCI procedure. A more detailed description of this method and a comparison of our entropy data with other results can be found in Supplemental Material [39].

Results.—To illustrate the effect of the XC functional, we first restricted our calculations to the ideal entropy of mixing, which allows for a direct comparison to the earlier results of Lorenzen *et al.* [14] shown in Fig. 1. The demixing temperature is given as a function of the He fraction x for various pressures. Results using the vdW-DF are shown as points and the dot-dashed curves are
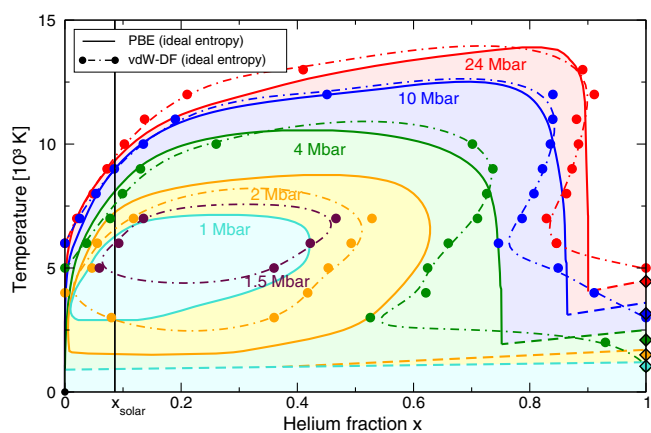
FIG. 1. Miscibility diagram of H-He mixtures for ideal entropy of mixing. Shown are the demixing temperatures as a function of the He fraction x for different pressures. The colored area indicates the immiscible region according to Ref. [14], where thick dashed lines indicate a possible liquidus line. The colored points are our results with the vdW-DF and ideal entropy of mixing; dot-dashed lines are guides to the eye. Colored diamonds show the melting temperatures of He for the color-coded pressure.

smoothing splines acting as a guide to the eye. The smoothing splines have been restricted to show a maximum between the highest T, where demixing occurs, and the next higher T, so that the critical point can only be estimated within 1000 K. For pressures of 24 and 10 Mbar we obtain similar demixing temperatures compared to PBE, especially for lower He fractions. Differences are more pronounced for higher He fractions. The PBE results show a vertical edge in the demixing temperatures at a He fraction of 0.9 for 24 Mbar and 0.86 for 10 Mbar, while our vdW-DF results show a tilt towards lower He fractions. At lower temperature, a kink appears where the demixing region extends to higher He fractions, and a complete separation into the pure components occurs below a certain temperature. Comparing these temperatures to the melting temperatures of He (colored diamonds at $x = 1$) results in good agreement.

For lower pressures the demixing region exhibits an island structure, where the islands are well separated from the possible liquidus line (dashed) at lower temperatures. The 2 Mbar demixing region is significantly smaller for the vdW-DF compared to PBE and we do not see demixing at pressures below 1.5 Mbar. This indicates that the vdW-DF shifts the miscibility diagram to higher pressures by 0.5 Mbar compared to PBE. It is known that the PBE functional underestimates the band gap. In liquid hydrogen, the underestimated band gap leads to metallization at too low pressures compared to the experiment of Knudson et al. [17]. In the PBE miscibility diagram this leads to demixing at too low pressures and thus too high temperatures in the low-pressure region. The vdW-DF improves the band gap of hydrogen so that metallization occurs at higher pressures more in agreement with the experiment of Knudson et al., which is also reflected in the miscibility diagram. Despite this progress, it remains a source of uncertainty if the vdW-DF predicts the actual band gap right, which has a direct influence on the low-pressure demixing diagram. Still, the overall similarity of the PBE and vdW-DF immiscibility region drives the conclusion that the general property of H-He insolubility is robust with respect to the chosen XC functional. To avoid the approximation of the ideal entropy of mixing, we performed coupling-constant integrations together with thermodynamic integration via the equation of state to assess nonideal effects in the entropy; see Supplemental Material for detail [39]. In Fig. 2 we show the miscibility diagram with the vdW-DF and compare the influence of entropy. Solid lines show smoothing splines corresponding to the colored circles, similar to Fig. 1. The inclusion of nonideal effects in entropy has four main consequences. First, the demixing temperatures are lowered significantly at high pressures and low He fractions. This consequence is particularly important for Jupiter and Saturn, whose mean He content is similar to the solar He abundance. Second, the demixing region now extends to smaller pressures than 1.5 Mbar,
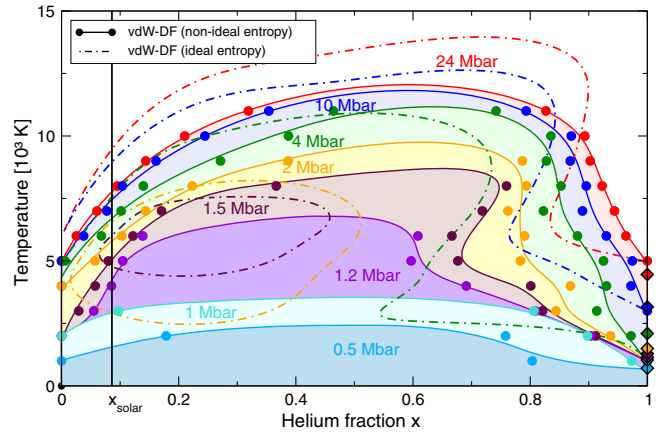
FIG. 2. Miscibility diagram of H-He mixtures for the vdW-DF. The points and colored areas indicate the immiscible region using the vdW-DF and nonideal entropy. Dot-dashed lines are our results with the ideal entropy of mixing as in Fig. 1. The vertical black line indicates the value of solar He concentration as relevant for Fig. 3. Colored diamonds show the melting temperatures of pure He at pressures indicated by the color code.

which directly removes the islandlike structure that appeared when using the ideal entropy. Third, the kink at high He fractions in the ideal entropy calculations is smoothed out at pressures above 2 Mbar. At pressures of 1.5 and 1.2 Mbar there is still a small sign of this effect. Fourth, the size of the demixing region is increased especially for high He fractions and low pressures. If demixing occurs in a planet, this significantly increases the amount of He in the He-rich droplets compared to the ideal entropy case. We estimate the uncertainty of the miscibility gap to be $\delta x = \pm 0.02$ due to errors in the underlying DFT-MD data and the Redlich-Kister fit of ΔG.

In Fig. 3 we show the miscibility diagram for the mean solar He concentration $x_{\text{solar}} = 0.086$, which is relevant for Jupiter and Saturn. We compare the miscibility regions obtained with PBE and the vdW-DF each for both ideal and nonideal entropy of mixing. Error bars are shown for the vdW-DF results for the nonideal entropy case only. These error bars have been determined from the data points in Fig. 2 for a maximum error of $\delta x = \pm 0.02$ in the helium fraction. The error is added and subtracted to the miscibility diagram in Fig. 2, so that the demixing temperature at x_{solar} is shifted, thus translating into error bars for the temperature.

For low pressures diamond anvil cell (DAC) results by Loubeyre et al. [42] exist. The orange points indicate the PBE demixing region with ideal entropy according to Lorenzen et al. In our vdW-DF calculations using the ideal entropy of mixing, we observe a similar shape of this region, which is a direct consequence of the island structure in Fig. 1. As noted before, the vdW-DF shifts demixing pressures upwards by 0.5 Mbar, which results in lower demixing temperatures at pressures smaller than 10 Mbar. Morales et al. also calculated the nonideal entropy using a coupling-constant integration and showed that a significant
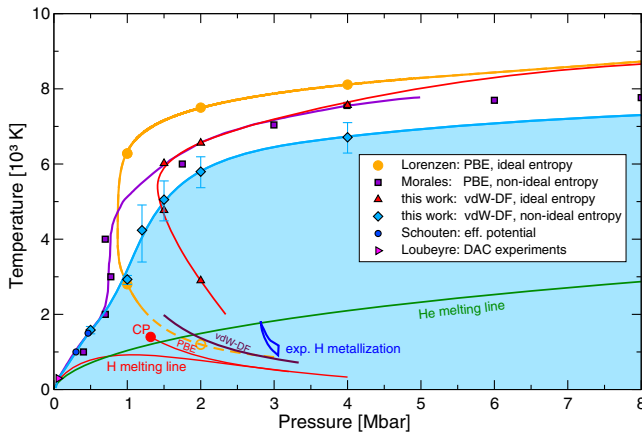
FIG. 3. Miscibility diagram at mean solar He abundance. Diamonds and the colored area show our vdW-DF results using the nonideal entropy; upward triangles are ideal entropy. Also shown are PBE data with ideal entropy [20] (orange circles) and nonideal entropy [15,16] (violet rectangles and the corresponding line). Small blue circles are from Schouten et al. [41]. The right pointing triangle is from DAC measurements [42]. For low temperatures melting lines for H and He and the nonmetal-to-metal phase transition in liquid hydrogen from PBE calculations, vdW-DF calculations [17], and experiments [17] are shown for orientation.

decrease in demixing temperature of at least 1000 K is obtained compared to the ideal entropy calculation of Lorenzen et al. In our calculations using the vdW-DF we also observe a lowering of the demixing temperature by 1000–2000 K when including the nonideal entropy. The influence of nonideal entropy on the enthalpy of mixing leads to a completely different low-pressure and low-temperature behavior than in the ideal entropy case. The demixing pressure decreases with decreasing temperature due to the removal of the island structure, cf., Fig. 2. For low pressures our results are in excellent agreement with calculations by Schouten et al. [41]. Thus, we derived a demixing line that perfectly connects our data to that of Schouten et al. and Loubeyre et al. [42].

In Fig. 4 we show isentropes for Jupiter and Saturn in comparison to our new demixing phase diagram. A value for Jupiter's entropy has been given in Ref. [38]: $s = 7.0782 \, k_B/\text{electron} = 7.613 k_B/\text{atom}$ for a mixture with He fraction $x = 0.07563$. We performed additional DFT-MD simulations using 256 electrons at the same He fraction to provide high accuracy data for the calculation of a vdW-DF isentrope. From our CCI entropy data, we determined the pressure and temperature for the given entropy value. This vdW-DF isentrope is shifted to higher pressures compared to the PBE isentrope of Militzer et al. [43] such that it intersects with the error bars of our miscibility diagram. An extension of this isentrope to lower pressures is, in principle, possible, but the additional simulations that are required at low densities are beyond the scope of this work. The Jupiter isentropes of Nettelmann et al. [44] and
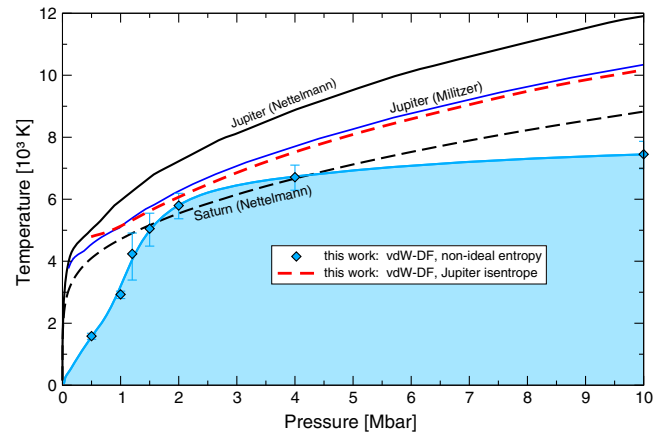
FIG. 4. Planetary isentropes in comparison to our miscibility diagram. Present-day isentropes for Jupiter [43,44] (black and blue solid line) and Saturn [45] (dashed black line) are indicated. Our vdW-DF isentrope is shown as a red dashed line.

Militzer et al. [43] do not cross our new demixing line while Saturn's isentrope still intersects with the miscibility region. We expect that a vdW-DF isentrope for Saturn would be shifted to higher pressures in a similar way as the vdW-DF Jupiter isentrope.

Discussion.—The combination of the vdW-DF and non-ideal entropy lowers the demixing temperatures to such an extent that the Jupiter isentrope of Nettelmann et al. [37] and even the substantially cooler isentrope of Militzer et al. [43] are completely outside of the immiscibility region; see Fig. 4. A corresponding preliminary Jupiter model was proposed recently [46]. Only our vdW-DF isentrope allows a minimal amount of demixing, if the error bars are taken into account. If demixing still occurs, it remains to be seen if planetary evolution models with helium rain are still able to reproduce the observed helium fraction in the atmosphere. The occurrence of hydrogen-helium immiscibility in Jupiter should therefore be critically discussed and the possibility of no helium rain at all should be taken into account. Other factors than demixing could influence the amount of He in the atmosphere. It has been suggested that molecular hydrogen might have such low opacity that a radiative zone may develop [47,48]. This zone could act as a barrier to convection, so that the combined effect of gravitational settling and thermal diffusion leads to a depletion of helium. Interestingly, the atmospheric helium abundance in the Sun is similar to that of Jupiter and this He depletion compared to the protosolar value is actually caused by gravitational settling and thermal diffusion [49]. However, it is still uncertain if a radiative zone does actually exist in Jupiter, because the opacity profile depends crucially on the abundance of heavy elements like sodium and potassium as well as titanium oxide [50]. The small neon abundance found in Jupiter, which has been linked to helium rain, might alternatively be explained in a clathrate-hydrate formation scenario where neon is not

easily trapped in these ice cages [51]. For the shown Saturn isentrope only a small fraction of the planet would lie inside the new demixing region. This implies that Saturn enters the demixing region at a later time than predicted from PBE calculations, which eventually reduces the cooling time to values below the age of the Solar System. On the other hand, the He fraction of the He-rich droplets will be significantly increased compared to PBE, leading to a substantially higher amount of He raining towards the interior and thus increasing compositional gradients. Leconte and Chabrier [52] pointed out that these gradients could lead to layered convection, which reduces the cooling rate of Saturn significantly and offers an alternative explanation for its excess luminosity. Since Militzer *et al.* found a substantially cooler Jupiter isentrope than Nettelmann *et al.*, we believe that a cooler Saturn isentrope remains possible, resulting in a larger demixing region. The miscibility diagram presented in this work sets important new constraints on planetary isentropes and thermal evolution tracks and enables the treatment of Saturn's luminosity problem in future work. Our data for the vdW-DF miscibility gap with nonideal entropy are available in Supplemental Material [39].

---

[*]manuel.schoettler@uni-rostock.de

[1] B. J. Conrath, D. Gautier, R. A. Hanel, and J. S. Hornstein, Astrophys. J. **282**, 807 (1984).

[2] U. Zahn, D. M. Hunten, and G. Lehmacher, J. Geophys. Res. Planets **103**, 22815 (1998).

[3] D. J. Stevenson, Phys. Rev. B **12**, 3999 (1975).

[4] B. J. Conrath and D. Gautier, Icarus **144**, 124 (2000).

[5] C. R. Proffitt, Astrophys. J. **425**, 849 (1994).

[6] D. J. Stevenson and E. E. Salpeter, Astrophys. J. Suppl. Ser. **35**, 221 (1977).

[7] J. J. Fortney, Science **305**, 1414 (2004).

[8] R. Püstow, N. Nettelmann, W. Lorenzen, and R. Redmer, Icarus **267**, 323 (2016).

[9] J. J. Fortney and W. B. Hubbard, Icarus **164**, 228 (2003).

[10] H. B. Niemann, S. K. Atreya, G. R. Carignan, T. M. Donahue, J. A. Haberman, D. N. Harpold, R. E. Hartle, D. M. Hunten, W. T. Kasprzak, P. R. Mahaffy, T. C. Owen, N. W. Spencer, and S. H. Way, Science **272**, 846 (1996).

[11] H. F. Wilson and B. Militzer, Phys. Rev. Lett. **104**, 121101 (2010).

[12] J. E. Klepeis, K. J. Schafer, T. W. Barbee, and M. Ross, Science **254**, 986 (1991).

[13] O. Pfaffenzeller, D. Hohl, and P. Ballone, Phys. Rev. Lett. **74**, 2599 (1995).

[14] W. Lorenzen, B. Holst, and R. Redmer, Phys. Rev. Lett. **102**, 115701 (2009).

[15] M. A. Morales, S. Hamel, K. Caspersen, and E. Schwegler, Phys. Rev. B **87**, 174105 (2013).

[16] M. A. Morales, E. Schwegler, D. Ceperley, C. Pierleoni, S. Hamel, and K. Caspersen, Proc. Natl. Acad. Sci. U.S.A. **106**, 1324 (2009).

[17] M. D. Knudson, M. P. Desjarlais, A. Becker, R. W. Lemke, K. R. Cochrane, M. E. Savage, D. E. Bliss, T. R. Mattsson, and R. Redmer, Science **348**, 1455 (2015).

[18] M. Dion, H. Rydberg, E. Schröder, D. C. Langreth, and B. I. Lundqvist, Phys. Rev. Lett. **92**, 246401 (2004).

[19] K. Lee, É. D. Murray, L. Kong, B. I. Lundqvist, and D. C. Langreth, Phys. Rev. B **82**, 081101 (2010).

[20] W. Lorenzen, B. Holst, and R. Redmer, Phys. Rev. B **84**, 235109 (2011).

[21] K. Ohta, K. Ichimaru, M. Einaga, S. Kawaguchi, K. Shimizu, T. Matsuoka, N. Hirao, and Y. Ohishi, Sci. Rep. **5**, 12743 (2015).

[22] M. Zaghoo, A. Salamat, and I. F. Silvera, Phys. Rev. B **93**, 155128 (2016).

[23] G. Mazzola, R. Helled, and S. Sorella, Phys. Rev. Lett. **120**, 025701 (2018).

[24] M. D. Knudson and M. P. Desjarlais, Phys. Rev. Lett. **118**, 035501 (2017).

[25] R. C. Clay III, M. Holzmann, D. M. Ceperley, and M. A. Morales, Phys. Rev. B **93**, 035121 (2016).

[26] O. Redlich and A. T. Kister, Ind. Eng. Chem. **40**, 345 (1948).

[27] F. Soubiran, S. Mazevet, C. Winisdoerffer, and G. Chabrier, Phys. Rev. B **87**, 165114 (2013).

[28] G. Kresse and J. Hafner, Phys. Rev. B **47**, 558 (1993).

[29] G. Kresse and J. Furthmüller, Phys. Rev. B **54**, 11169 (1996).

[30] G. Kresse and J. Furthmüller, Comput. Mater. Sci. **6**, 15 (1996).

[31] J. Klimeš, D. R. Bowler, and A. Michaelides, J. Phys. Condens. Matter **22**, 022201 (2010).

[32] J. Klimeš, D. R. Bowler, and A. Michaelides, Phys. Rev. B **83**, 195131 (2011).

[33] G. Kresse and D. Joubert, Phys. Rev. B **59**, 1758 (1999).

[34] A. Baldereschi, Phys. Rev. B **7**, 5212 (1973).

[35] W. G. Hoover, Phys. Rev. A **31**, 1695 (1985).

[36] P. H. Berens, D. H. J. Mackay, G. M. White, and K. R. Wilson, J. Chem. Phys. **79**, 2375 (1983).

[37] N. Nettelmann, A. Becker, B. Holst, and R. Redmer, Astrophys. J. **750**, 52 (2012).

[38] B. Militzer, Phys. Rev. B **87**, 014202 (2013).

[39] See Supplemental Material http://link.aps.org/supplemental/10.1103/PhysRevLett.120.115703, which includes Refs. [16,26,38,40], for details on the calculation of entropies and data tables of the miscibility gap.

[40] F. Soubiran and B. Militzer, Astrophys. J. **829**, 14 (2016).

[41] J. A. Schouten, A. de Kuijper, and J. P. J. Michels, Phys. Rev. B **44**, 6630 (1991).

[42] P. Loubeyre, R. LeToullec, and J. P. Pinceaux, J. Phys. Condens. Matter **3**, 3183 (1991).

[43] B. Militzer and W. B. Hubbard, Astrophys. J. **774**, 148 (2013).

[44] N. Nettelmann, B. Holst, A. Kietzmann, M. French, R. Redmer, and D. Blaschke, Astrophys. J. **683**, 1217 (2008).

[45] N. Nettelmann, R. Püstow, and R. Redmer, Icarus **225**, 548 (2013).

[46] W. B. Hubbard and B. Militzer, Astrophys. J. **820**, 80 (2016).

[47] T. Guillot, D. Gautier, G. Chabrier, and B. Mosser, Icarus **112**, 337 (1994).

[48] T. Guillot, Icarus **112**, 354 (1994).

[49] J. N. Bahcall and M. H. Pinsonneault, Astrophys. J. **395**, L119 (1992).

[50] T. Guillot, D. J. Stevenson, W. B. Hubbard, and D. Saumon, in *Jupiter. The Planet, Satellites and Magnetosphere*, edited by F. Bagenal, T. E. Dowling, and W. B. McKinnon (Cambridge University Press, Cambridge, 2004), pp. 35–57.

[51] P. Irwin, *Giant Planets of our Solar System*, 2nd ed. (Springer-Verlag, Berlin Heidelberg, 2009).

[52] J. Leconte and G. Chabrier, Nat. Geosci. **6**, 347 (2013).